



## 1 **Dynamics of short-term ecosystem carbon fluxes induced by** 2 **precipitation events in a semiarid grassland.**

3 Josué Delgado-Balbuena<sup>1</sup>, Henry W. Loescher<sup>2,3</sup>, Carlos A. Aguirre-Gutiérrez<sup>1</sup>, Teresa  
4 Alfaro-Reyna<sup>1</sup>, Luis F. Pineda-Martínez<sup>4</sup>, Rodrigo Vargas<sup>5</sup>, and José T. Arredondo<sup>6</sup>.

5 <sup>1</sup>Centro Nacional de Investigación Disciplinaria Agricultura Familiar, INIFAP, km 8.5 Carr. Ojuelos – Lagos  
6 de Moreno, 47563, Ojuelos de Jalisco, Jal., México

7 <sup>2</sup>Battelle, National Ecological Observatory Network (NEON), Boulder, CO USA 80301,

8 <sup>3</sup>Institute of Alpine and Arctic Research (INSTAAR), University of Colorado, Boulder, CO USA 80301.

9 <sup>4</sup>Universidad Autónoma de Zacatecas, 108 Calzada Universidad, 98066 Zacatecas, Zacatecas, Mexico

10 <sup>5</sup>Department of Plant and Soil Sciences, University of Delaware, Newark, DE, USA

11 <sup>6</sup>Division de Ciencias Ambientales, Instituto Potosino de Investigación Científica y Tecnológica, Camino a la  
12 Presa de San José 2055, Lomas 4ta, 78216 San Luis Potosí, S.L.P., México.

13

14 *Correspondence to:* Josué Delgado-Balbuena (delgado.josue@inifap.gob.mx)

15 **Abstract.** Precipitation (PPT) patterns in semiarid grasslands are characterized by infrequent and small PPT  
16 events; however, plants and soil microorganisms are adapted to use the unpredictable small pulses of water.  
17 Several studies have shown short-term responses of carbon and nitrogen mineralization rates (called the  
18 priming effect or the Birch effect) stimulated by wet-dry cycles; however, dynamics, drivers, and the  
19 contribution of the “priming effect” to the annual C balance is poorly understood. Thus, we analysed six years  
20 of continuous net ecosystem exchange measurements to evaluate the effect of the PPT periodicity, magnitude  
21 of individual PPT events on the daily/annual ecosystem C balance (NEE) in a semiarid grassland. We  
22 included the period between PPT events, a priori daytime NEE rate and a priori soil moisture content as the  
23 main drivers of the priming effect. Ecosystem respiration (ER) responded within few hours following a PPT  
24 event whereas it took five-nine days for gross ecosystem exchange (GEE; such as  $-NEE = GEE + ER$ ) to  
25 respond. Precipitation events as low as 0.25 mm increased ER, but cumulative PPT > 40 mm that infiltrated  
26 deep into the soil profile stimulated GEE. Overall, ER fluxes following PPT events were related to the change  
27 of soil water content at shallow depth and previous soil conditions (e.g., previous NEE rate, previous soil  
28 water content) and the size of the stimulus (e.g., PPT event size). Carbon effluxes from priming effect  
29 accounted for less than 5% of ecosystem respiration but were significantly high respect to the carbon  
30 balance. In the long-term, changes in PPT regimes to more intense and less frequent PPT events, as expected  
31 by the climate change effect, could convert the semiarid grassland from a slight C sink to a C source.

32 **Keywords:** Eddy covariance, net ecosystem exchange, ecosystem respiration, *Bouteloua gracilis*, blue grama,  
33 priming effect, Birch effect.

34



## 35 1. Introduction

36 Arid lands comprise a wide range of ecosystem types covering more than 30% of terrestrial land (Lal, 2004).  
37 In these ecosystems annual potential evapotranspiration is larger than annual precipitation due to regional  
38 atmospheric high-pressure zones (Hadley cells), continental winds, cold oceanic winds and local orographic  
39 effects that reduce the precipitation amounts (Maliva and Missimer, 2012). Here, precipitation (PPT) occurs  
40 as infrequent, discrete, small (< 5 mm) and unpredictable events (Noy-Meir, 1973; Loik et al, 2004). This  
41 results in water-limited ecosystems, where biological activity is restricted to periods of soil water availability  
42 (Lauenroth and Sala, 1992). Consequently, the productivity and stability of these ecosystems are more  
43 vulnerable to changes in climate, particularly to changes of the historic mean annual PPT (MAP) amounts and  
44 the change in the periodicity (frequency) of these PPT events.

45 Precipitation stimulates short-term changes of carbon and nitrogen mineralization rates because soil  
46 microorganisms activate with the increase of soil water content (Turner and Haygarth, 2001). This “priming  
47 effect” (Borken and Matzner, 2009) also called the Birch effect (Birch, 1964), describes the soil carbon  
48 released from decomposition of heterotrophic sources to the atmosphere following soil rewetting. Amount  
49 and timing of PPT events modify the magnitude and duration of the priming effect by modulating soil wet-dry  
50 cycles. The size of a PPT event determines the temporal duration and the biotic components that respond to  
51 the pulse (Huxman et al., 2004a), and thus, defines the magnitude and direction of CO<sub>2</sub> effluxes (Chen et al.,  
52 2009). In general, small precipitation events that induce changes in soil humidity at shallow depth do not  
53 induce plant activity, but activate soil microorganisms (Collins et al., 2008). On the other hand, successive  
54 rewetting cycles reduce carbon mineralization rates as the amount of available organic labile carbon declines  
55 (Jarvis et al., 2007). Thus, PPT events after long drought periods (until nine months in semiarid grasslands)  
56 trigger larger and longer soil respiration efflux rates compared to consecutive PPT events (Reichmann et al.,  
57 2013).

58 At the ecosystem scale, deserts and grasslands have shown larger CO<sub>2</sub> efflux rates after rewetting than  
59 temperate ecosystems or croplands (Kim et al., 2012), and in ecosystems with low soil organic carbon content  
60 (Bastida et al., 2019). Characteristics and dynamics of these short-term soil C effluxes were addressed by the  
61 “Threshold-Delay” model (T-D model, Ogle and Reynolds 2004). The T-D model take the previous  
62 environmental conditions, PPT event size, PPT thresholds, and time-delays to inform the time constants that  
63 modulate ecosystem responses after a PPT event. Moreover, Huxman et al., (2004a) described the dynamics  
64 of the net ecosystem exchange of carbon (NEE) and its components (gross ecosystem exchange = GEE, and  
65 ecosystem respiration = ER, such as  $-NEE = GEE + ER$ ) with parameters of the T-D model (Fig. A1). GEE  
66 and ER have different time delays based on threshold PPT quantities and event size, with ER responding to  
67 smaller PPT events than GEE (Huxman et al. 2004a). In addition, both GEE and ER have asymptotic  
68 responses to large PPT events (the upper PPT thresholds), with an upper ER threshold lower than that found  
69 for the GEE threshold (Huxman et al. 2004).

70 In the semiarid grasslands of Mexico, small PPT events are likely to activate biological soil crusts (BSC) on  
71 the soil surface that cover up to 60% of plant interspaces (Concostrina-Zubiri et al., 2014), and to stimulate



72 ER instead of C uptake. However, *Bouteloua gracilis* H.B.K. Lag ex Steud (blue grama), the keystone  
73 species in the semiarid grassland of Mexico (Medina-Roldán et al., 2007) may contribute to C uptake because  
74 of its adaptations to take advantage of smaller PPT events (Sala and Lauenroth, 1982, Medina-Roldán et al.,  
75 2013). Understanding disturbances of ecosystem processes (C fluxes) due to changing regional PPT pattern  
76 in semiarid grasslands is particularly salient given that the global circulation models forecast a 10% to a 30%  
77 reduction of summer and winter precipitation, respectively at the end of the 21<sup>st</sup> Century (Christensen et al.,  
78 2007), and the PPT patterns is forecasted to have fewer events with more water quantity per event (Easterling  
79 et al., 2000).

80 Thus, the objective of this study was to evaluate the effect of PPT periodicity and magnitude of individual  
81 PPT events and a priori soil moisture conditions on daily and annual ecosystem C balance (NEE) for the  
82 semiarid grassland in Mexico. Over a six-year study period, we examined event-based PPT amount, the  
83 period between PPT events, a priori daytime NEE rate and a priori soil water content at two depths as the  
84 main drivers of daily mean NEE change rate. Because we were interested on short-term NEE change and its  
85 components, only short-term NEE change within few days following a PPT event were evaluated. Effects on  
86 daily mean GEE ( $GEE = -NEE + ER$ ) was also evaluated at the beginning of the growing season. Based on  
87 the T-D model (Ogle and Reynolds, 2004), we expect that; 1) semiarid grassland will exhibit a quick response  
88 (short time-delay) to small PPT events (Low PPT threshold) through positive NEE fluxes (C release, H1).  
89 Moreover, 2) ER and GEE (C release and C uptake, respectively) will differ in their time response and PPT  
90 thresholds, with shorter time-delays and lower PPT thresholds for ER than GEE (H2). This response is  
91 because of small PPT events should enhance ER mainly through heterotrophic respiration of soil surface  
92 microorganisms that are activated within one hour after wetting (Placella et al., 2012), whereas larger PPT  
93 events are required to reach roots at deeper soil profiles and that plants need longer times for start growing.  
94 On the other hand, we expect that, 3) size and timing of PPT patterns will modulate the magnitude of C  
95 efflux; therefore, large precipitation events after long dry periods will release more CO<sub>2</sub> than small or  
96 consecutive PPT events (H3). Finally, we expect, 4) C efflux after PPT events will be a meaningful CO<sub>2</sub>  
97 source to the atmosphere in the semiarid grassland which will decrease the annual net C uptake of the  
98 ecosystem (H4).

## 99 2. Materials and methods

### 100 2.1 Site description

101 The study site is located on a shortgrass steppe, within the Llanos de Ojuelos subprovince of Jalisco state,  
102 Mexico. The shortgrass biome in Mexico extends from the North American Midwest along a strip that  
103 follows the Sierra Madre Occidental through the Chihuahuan Desert into the sub-province Llanos de Ojuelos.  
104 Vegetation is dominated by grasses, with *Bouteloua gracilis* (Willd. ex Kunth) Lag. ex Griffiths as the key  
105 grass species, forming near mono-specific stands. The region has a semiarid climate with mean annual  
106 precipitation of 424 mm ± 11 mm (last 30 years, Delgado-Balbuena et al., 2019) distributed mainly between  
107 June and September and with 6 to 9 months of no rain. Winter-summer rain accounts for < 20% of the total



108 annual precipitation (Delgado-Balbuena et al., 2019). Mean annual temperature is  $17.5 \pm 0.5$  °C. The  
109 topography is characterized by valleys and gentle rolling hills with soils classified as haplic xerosols  
110 (associated with lithosols and eutric planosols), and haplic phaeozems (associated with lithosols) (Aguado-  
111 Santacruz, 1993). Soils are shallow with average depth of 0.3-0.4 m containing a cemented layer at  $\sim 0.5$  m  
112 deep, with textures dominated by silty clay and sandy loam soils (Aguado-Santacruz, 1993).  
113 The study site is a fenced area of  $\sim 64$  ha of semiarid grassland under grazing management. A 6 m high tower  
114 was placed at the center of the area of interest to support carbon-energy flux measurements and  
115 meteorological instruments as well. That location allowed an ever-changing and integrated measurement  
116 footprint of 320 m, 410 m, 580 m, and 260 m from the tower according to the N, E, S, and W orientations,  
117 respectively.

## 118 2.2 Meteorological and soil measurements

119 Meteorological data was collected continuously at a rate of 1 s and averaged at 30 min intervals using a  
120 datalogger (CR3000, Campbell Scientific Inc., Logan, Utah). Variables measured included air temperature  
121 and relative humidity (HMP45C, Vaisala, Helsinki, Finland) housed into a radiation shield (R.M. Young  
122 Company Inc., Traverse City, MI), incident and reflected shortwave and longwave solar radiation (NR01,  
123 Hukseflux, Netherlands), and photosynthetic photon flux density (PPFD, PAR lite, Kipp and Zonen, Delft, the  
124 Netherlands). Soil variables were measured at a 5 min frequency and averaged at 30 min intervals. These  
125 included volumetric soil water content (CS616, Campbell Sci., Logan, UT) positioned horizontally to 2.5 cm  
126 and 15 cm deep, average soil temperature of the top 8 cm soil profile, and soil temperature at 5 cm deep  
127 (T108 temperature probes, Campbell Scientific Inc., Logan, UT). Soil temperature variables were acquired  
128 with another datalogger (CR510, Campbell Scientific Inc., Logan, UT). Precipitation was measured with a  
129 bucket rain gauge installed 5 m away from the tower (FTS, Victoria, British Columbia, Canada) at 1 m.a.g.l.

## 130 2.3 Net ecosystem CO<sub>2</sub> exchange measurements

131 An open path eddy covariance system was placed at 3 m high to cover a fetch of 300 m and used to measure  
132 NEE over the semiarid grassland. The system consisted of a three-dimensional sonic anemometer (CSAT-3D,  
133 Campbell Sci., Logan, UT) for measuring wind velocity on each polar coordinate ( $u$ ,  $v$ ,  $w$ ) and sonic  
134 temperature ( $\theta_s$ ), and an open-path infrared gas analyzer (IRGA, Li-7500, LI-COR Inc., Lincoln, NE) to  
135 measure CO<sub>2</sub> and water vapor concentrations. Instruments were mounted in a tower at 3 m above the soil  
136 surface oriented towards the prevailing winds. The IRGA sensor was mounted next to—and 10 cm offset from  
137 the anemometer transducers, the center of the IRGA optical path was centered with the distance between the  
138 vertically oriented sonic transducers and tilted 45° to avoid dust and water accumulation in the IRGA optical  
139 path. Digital signal of both sensors was recorded at a sampling rate of 10 Hz in a datalogger (CR3000,  
140 Campbell Scientific Inc., Logan, UT) (Ocheltree and Loescher 2007). NEE was estimated as:

$$141 \quad NEE = \overline{w'CO_2'} \quad (1)$$



142 overbar denotes time averaging and primes are the deviations of instantaneous values (at 10 Hz) from a block-  
143 averaged mean (30 min) of vertical windspeed ( $w$ ,  $\text{m s}^{-1}$ ) and molar volume of  $\text{CO}_2$  ( $\mu\text{mol CO}_2 \text{ m}^{-3}$ ),  
144 respectively. Micrometeorological convention was used, where negative NEE values stand for ecosystem C  
145 uptake (Loescher et al., 2006). We did not estimate a storage flux because of the low vegetation stature and  
146 well mixed conditions; therefore, we assumed it would be 0 over a 24-h period (Loescher et al., 2006).

#### 147 **2.4 Data processing**

148 Raw eddy covariance data were processed in EdiRe (v1.5.0.10, University of Edinburgh, Edinburgh UK).  
149 Wind velocities, sonic temperature,  $[\text{CO}_2]$ , and  $[\text{H}_2\text{O}]$  signals were despiked, considering outliers those values  
150 with a deviation larger than  $\pm 8$  standard deviations. A 2-D coordinate rotation was applied to sonic  
151 anemometer wind velocities to obtain turbulence statistics perpendicular to the local streamline. Lags  
152 between horizontal wind velocity and scalars were removed with a cross-correlation procedure to maximize  
153 the covariance among signals. Carbon and water vapor fluxes were estimated as molar fluxes ( $\text{mol m}^{-2} \text{ s}^{-1}$ ) at  
154 30 min block averages, and then they were corrected for air density fluctuations (WPL correction, Webb et al.  
155 1980). Frequency response correction was done after Massman (2000). Sensible heat flux was estimated  
156 from the covariance between fluctuations of horizontal wind velocity ( $w'$ ) and sonic temperature ( $\theta'_s$ ). This  
157 buoyancy flux was corrected for humidity effects (Schotanus et al. 1983, Foken et al., 2012).

158 Fluxes were submitted to quality control procedures, i) stationarity ( $<50\%$ ), ii) integral turbulence  
159 characteristics ( $<50\%$ ), iii) flags of IRGA and sonic anemometer (AGC value  $<75$ , Max CSAT diagnostic flag  
160 = 63) which are strongly related with advices of problem measurement due to rain events, iv) screening of  
161 flux values into a logical magnitudes ( $\pm 20 \mu\text{mol CO}_2 \text{ m}^{-2} \text{ s}^{-1}$ ), and v) a threshold  $u^* = 0.1 \text{ m s}^{-1}$  was used to  
162 filter nighttime NEE under poorly developed turbulence. This threshold was defined through the 99%  
163 threshold criterion after Reichstein et al. (2005).

164 Temporally integrated estimates are noted throughout this paper. Because of GEE cannot be measured  
165 directly, it was estimated by ER withdrawal from -NEE. The ER was estimated in two ways, 1) it was  
166 estimated from light-response curves (see below), and 2) it was determined from nighttime NEE data (under  
167  $\text{PPFD} < 10 \mu\text{mol m}^{-2} \text{ s}^{-1}$  light conditions). Different ER estimation method is indicated throughout the paper.

168 For identifying changes induced by PPT events on GEE and ER, daytime and nighttime NEE data on a one  
169 day-window was adjusted with a rectangular hyperbolic response function to photosynthetic photon flux  
170 density (PPFD; Ruimy et al. 1995).

$$171 \quad NEE = \frac{\alpha \cdot \text{PPFD} \cdot A_{max}}{\alpha \cdot \text{PPFD} + A_{max}} + ER \quad (2)$$

172 where,  $\alpha$  is the apparent quantum yield ( $\mu\text{mol CO}_2 \text{ m}^{-2} \text{ s}^{-1} / \mu\text{mol CO}_2 \text{ m}^{-2} \text{ s}^{-1}$ ),  $A_{max}$  is maximum  
173 photosynthetic capacity ( $\mu\text{mol CO}_2 \text{ m}^{-2} \text{ s}^{-1}$ ), and  $ER$  is the ecosystem respiration ( $\mu\text{mol CO}_2 \text{ m}^{-2} \text{ s}^{-1}$ ). Due to  
174  $A_{max}$  is calculated to unrealistic “infinite” PPFD, we calculated a more realistic maximum photosynthetic  
175 capacity ( $A_{2500}$ ), which is maximum photosynthesis at  $2500 \mu\text{mol m}^{-2} \text{ s}^{-1}$ . Changes and transitions from ER  
176 dominated NEE fluxes to C-gain processes (GEE) were verified with the shape of the light response curve.



## 177 2.5 Gap filling procedures and characterization of PPT events

178 Data gaps shorter than two hours were linearly interpolated, whereas gaps larger than two hours were left as  
179 empty data. Only daytime-NEE data were used for most of the analysis because of nighttime NEE is  
180 subjected to quality problems, which include poor developed turbulences caused few 30-min periods with  
181 available data and showed strong divergence from NEE averages if the whole night cycle is not similarly  
182 represented among days. Daily mean ER derived from nighttime NEE data were used for analysis when more  
183 than 50% of the data was available after QA/QC procedures. The NEE related PPT events were selected for  
184 analysis based on data quality and availability to evenly cover the daytime cycle (on average more than 85%  
185 of NEE data) and then averaged through the day. The daytime-scale was selected to avoid confounding  
186 diurnal NEE variability and to achieve robust analyses. All precipitation events between 2011 and 2016 were  
187 isolated and then filtered by the number of half-hours accounted for mean daily fluxes.

188 The C flux one day before the PPT event was taken as the reference C flux. Event-response effect (“priming  
189 NEE effect”) was measured as the difference between mean daytime NEE post-event and mean daytime NEE  
190 pre-event, such that.

$$191 \Delta\text{NEE} = \text{NEE}_{\text{post-event}} - \text{NEE}_{\text{pre-event}} \quad (3)$$

192 where, NEE is the daytime NEE average ( $\mu\text{mol m}^{-2} \text{s}^{-1}$ ).

193 The same method was used to calculate changes of soil water content at 2.5 and 15 cm depth ( $\Delta\text{VWC}_{2.5}$  and  
194  $\Delta\text{VWC}_{15}$ , respectively), and change of photosynthetic photon flux density ( $\Delta\text{PPFD}$ )

195 Intervals between PPT events (hereafter inter-event periods, IEP) were counted in days from the last PPT  
196 event, regardless of its magnitude.

197 Enhanced vegetation index (EVI) of 250 m spatial resolution and 8 day time-resolution from NASA’s MODIS  
198 instruments was used as an approximation of plant leaf activity. The Savitzky-Golay (Yang et al., 2014) filter  
199 was used to eliminate outliers of EVI derived from adverse atmospheric conditions.

200 According to the model, where previous conditions are determinant of carbon fluxes, data were divided in  
201 “fluxes dominated by photosynthesis (carbon uptake)” and “fluxes dominated by ecosystem respiration  
202 (carbon efflux)”. A threshold of  $-1 \mu\text{mol m}^{-2} \text{s}^{-1}$  of average previous daytime  $\text{CO}_2$  flux was used to divide data.

203 This was done to avoid confounding factors, because of environmental drivers of photosynthesis and  
204 respiration may differ in magnitude and direction. Moreover, under photosynthetic conditions is hard to  
205 identify if a positive change of NEE (less photosynthesis) was due to an increase of soil respiration or a  
206 dampening of photosynthesis by less available radiation under cloudy conditions.

## 207 2.6 Statistical analysis

208 Boosted regression trees analysis (BRT; Elith and Leathwick, 2017) were developed to identify the most  
209 important variable controlling the priming C effect and thresholds of this response. BRT analysis also were  
210 used to identify the form of function, i.e., whether relationship between independent variables and the priming  
211 effect was linear, exponential, sigmoidal, peak from, etc. Independent variables included PPT event size, inter  
212 event-periods (IEP), a priori, current, and change of volumetric water content (VWC) at two depths (2.5 and



15 cm), soil temperature, previous daytime NEE, enhanced vegetation index (EVI) and change in photosynthetic photon flux density ( $\Delta$ PPFD). For BRT analysis, data was divided in “photosynthesis dominated” and “respiration dominated” data. On the other hand, for identify delays between C fluxes (ecosystem respiration and gross primary productivity) and precipitation events, a cross correlation analysis was done. For cross correlation, parameter of the light response curve was used; the ER was used to identify delays between ecosystem respiration and soil water content at 2.5 cm, and  $A_{2500}$  was used to identify delays between gross ecosystem productivity and soil water content at 15 cm, because of ER and  $A_{2500}$  were better correlated with soil volumetric water content at 2.5 and 15 cm, respectively. All these variables were detrended before cross-correlation analysis. Finally, linear correlation analyses were performed among environmental variables and priming effect and nighttime ER, and among independent variables to test for autocorrelations. The “gbm” package (The R core team) was used for performing BRT analysis, whereas the “astsa” package for R was used to conduct cross correlation analyses.

### 225 3. Results

#### 226 3.1 Precipitation pattern

227 Cumulative precipitation for 2011 (288.5 mm) was below the 30-y average for the site (420 mm) and was the  
228 worst drought of the last 70-y. In contrast, 2012 received less PPT (393.2 mm), and 2014 and 2016 received  
229 more PPT (528.5 and 436 mm, respectively) than average, whereas 2013 (601.6 mm) and 2015 (785.9 mm)  
230 were very humid years (Fig. 1). The 6-y differed in precipitation frequency, but they were similar in the size  
231 of PPT events with ~60% of the PPT events < 5 mm (Fig. 2a). However, notwithstanding the lower  
232 proportion of larger size PPT events (PPT events > 5 mm), they summed similar or even more amount of  
233 water than small PPT events (Fig. 2b). Overall, precipitation pattern was characterized by short inter event  
234 periods with 60% of PPT events falling consecutively (IEP < 5 days; Fig. 2c).

235 Soil saturated after large or recurrent PPT events. Largely, soil moisture was maintained over a 10% in the  
236 wettest years, with the largest peak reaching a 40% in summer 2014 (Fig. 1b). Most VWC variability was  
237 observed at 2.5 cm rather than 15 cm depth and it was better correlated with precipitation amount per event ( $p$   
238 < 0.05,  $R^2 = 0.72$ , Fig. 2d) increasing 0.3 % per mm of precipitation. PPT events of 0.25 mm increased the  
239  $VWC_{2.5}$  in ~1-2%, but this increase lasted for less than one hour, whereas  $VWC_{15}$  increased after PPT ~5 mm  
240 (data not shown). Additionally, PPT events and soil moisture dynamics at 15 cm depth were out of phase (up  
241 to five days between the PPT event and the  $SWC_{15}$  peak, Fig. 2e)

242 A total of 256 events from this 6-y study were used for statistical analysis. A sample of 100 PPT events was  
243 used for the respiration dominated fluxes ( $>-1.0 \mu\text{mol m}^{-2} \text{s}^{-1}$ ), and 156 PPT events for the photosynthesis  
244 dominated fluxes ( $>-1.0 \mu\text{mol m}^{-2} \text{s}^{-1}$ ). Small precipitation events dominated in our database but represented  
245 well the precipitation pattern of the site. The sample was integrated by events in the range from 0.25 to 57.1  
246 mm, and a mean of  $5.7 \pm 0.53$  mm (mean  $\pm$  1 SE). Large PPT events occurred after short inter-event periods,  
247 and small PPT events were preceded by long inter-event periods. Medium PPT events after long inter-event  
248 periods were rare, and extreme large PPT events after long inter-event periods were not observed (Fig. 2f).



249 The size of the precipitation event (PPT) and previous soil water content at 2.5 cm depth (preVWC<sub>2.5</sub>)  
250 explained a large variation of change in soil water content at 2.5 cm depth ( $\Delta\text{VWC}_{2.5}$ ;  $R^2 = 0.54$ ; Fig. 2d).  
251 Best correlation among variables was observed between previous soil water content and soil water content at  
252 different depths; for instance,  $\text{VWC}_{15}$  and pre  $\text{VWC}_{15}$  ( $R^2 = 0.84$ ), between the same variables but at 2.5 cm  
253 ( $R^2 = 0.81$ ). The change in NEE (priming effect) has not a strong relationship with any single variable (Fig.  
254 A2).

### 255 3.2 Time delays and thresholds.

256 The minimum PPT event that altered NEE rates was 0.25 mm. Overall, the analysis of half hour fluxes  
257 showed almost instantaneous positive response of NEE to PPT event that exponentially decreased over time  
258 into a half to two hours after the PPT event (Fig. A3). ER rates increased after 0.25 mm PPT events, but we  
259 detected a different threshold for GEE where either a larger PPT event or multiple consecutive events (*e.g.*, >  
260 40 mm, Fig. 2a) was needed, and showed a delay of ~5 days after the positive change in VWC at the 15 cm  
261 depth, this at the beginning of the growing season (Fig. 3a, b).

262 Cross-correlation analysis of light-response curve parameters showed no lags between ecosystem respiration  
263 (ER) and volumetric soil water content at 2.5 cm. (Fig. 3a), whereas there was a lag of 9 days between  
264 photosynthetic capacity at 2500 PPFD ( $A_{2500}$ ; Fig. 3b) and soil water content, which was larger than the  
265 observed at several precipitation events of 2013 (Fig. 2a,b).

266 The BRT analysis showed sigmoidal relationships between the priming effect and environmental variables  
267 with different thresholds. At the respiration-dominated period, a minimum change of soil volumetric water  
268 content at 2.5 cm affected positively the carbon flux, but a change larger than 8% in this variable did not  
269 induce a larger C efflux (upper threshold; Fig. 4). On the other hand, C priming effect was larger under  
270 neutral previous NEE (preNEE~0) and decreased in magnitude as preNEE becomes more positive (Fig. 5).  
271 Moreover, previous dry conditions at shallow soil depth promoted larger C efflux by the priming effect, and  
272 this effect decreased as soil previous conditions were wetter, with a threshold at 15% (Fig. 5). Similar to the  
273 change in soil water content at 2.5 cm, even the lowest PPT event (0.25 mm) caused an increase of C efflux,  
274 but with a threshold between 10 - 15 mm. Precipitation events larger than 15 mm did not enhanced the  
275 priming effect (Fig. 5). In contrast, in the photosynthesis dominated period, larger priming effect was  
276 observed at more negative preNEE ( $-7 \mu\text{mol m}^{-2} \text{s}^{-1}$ ) and had no more effect at  $\sim -4 \mu\text{mol m}^{-2} \text{s}^{-1}$ . The priming  
277 effect was enhanced by dry soil conditions at 15 cm depth (< 30%) with a rapid suppression after that. On the  
278 other hand, the priming effect was gradually decreasing with reductions of PPFD.

279 Nighttime NEE (ecosystem respiration) showed correlation with soil water content at the two depths and EVI;  
280 however, the relationship was linear at low soil water content, reached a maximum at medium values of VWC  
281 and then decreased with minimum values at high soil water content. The largest ecosystem respiration was  
282 observed at higher EVI values (Fig. A4)





### 283 3.3 Dynamics and drivers of the “Priming effect”

284 The priming effect lasted longer with initial larger change of NEE, i.e., whereas higher was the priming effect  
285 ( $\Delta$ NEE), the C fluxes lasted more time in returning to initial values (previous to PPT event); however,  
286 decreasing NEE rates were better explained by PPT event size than the initial change of NEE (insert Fig. 4).  
287 For instance, after a 13.7 mm PPT event and initial daytime NEE =  $5.1 \mu\text{mol m}^{-2} \text{s}^{-1}$ , the C flux exponentially  
288 decreased at a rate of  $\sim 50\%$  of its earlier value, whereas with an initial NEE efflux  $\sim 2.5 \mu\text{mol m}^{-2} \text{s}^{-1}$ , the C  
289 flux decreased at a rate of 100% (Fig. 4). Thus, total C efflux was a contribution of the initial change of NEE  
290 and the time taken to return to basal values (i.e., decreasing rates).

291 According to BRT analysis, the factor that most influenced the priming effect in the respiration-dominated  
292 period was the change of soil water content at 2.5 cm depth ( $\Delta$ VWC<sub>2.5</sub>; relative importance, RI = 18%), which  
293 was followed by the a priori NEE (preNEE; RI = 14%), the previous VWC at 2.5 cm depth (RI=14%) and the  
294 size of PPT event (RI = 13%). All the other factors had individual RI values lower than 10% (Table 1; Fig. 6).  
295 Maximum  $\Delta$ NEE values were observed at i) larger changes of soil water content at 2.5 cm depth (Fig. 6a), ii)  
296 previous neutral NEE (i.e., NEE  $\sim 0 \mu\text{mol m}^{-2} \text{s}^{-1}$ ; Fig. 6b), iii) previous dry soil water content at 2.5 cm depth  
297 (Fig. 6c), and iv) with large PPT events ( $>15 \text{ mm d}^{-1}$ ; Fig. 6d). The priming NEE effect decreased farther than  
298 these limits. In contrast, in the photosynthesis-dominated period, the previous NEE was the most important  
299 factor explaining the “priming effect” (RI=33%), whereas the volumetric water content at 15 cm depth, the  
300 change of photosynthetic photon flux density and the volumetric water content at 2.5 cm depth followed in  
301 importance (Table 1). Larger changes in NEE (priming effect) were observed at i) more negative previous  
302 NEE (i.e., under more photosynthetic activity; Fig. 6e), ii) under drier soil water conditions at 15 cm depth  
303 (Fig. 6f), iii) with larger changes of PPFD (decrease of PPFD; Fig. 6g), and iv) under air temperature lower  
304 than  $16^\circ\text{C}$  and higher than  $19^\circ\text{C}$  (Fig. 6h). There was a large interaction between preVWC<sub>2.5</sub> and PPT for  
305 the respiration-dominated period and between preNEE and  $\Delta$ PPF for the photosynthesis-dominated period.

### 306 3.4 Contribution of priming effect to carbon balance

307 The carbon balance for this six-year period for this site was of  $-126 \text{ g C m}^{-2}$ , with 2955 and  $-3080 \text{ g m}^{-2}$  of  
308 ecosystem respiration and gross ecosystem exchange, respectively, and varied from a sink of  $-107 \text{ g C m}^{-2} \text{ y}^{-1}$   
309 to a source of  $114 \text{ g C m}^{-2} \text{ y}^{-1}$  (Delgado-Balbuena et al., 2019). Roughly calculation of carbon efflux due to  
310 priming effect indicated that extrapolation of mean  $\Delta$ NEE per event and by year, contributes with  $142 \text{ g m}^{-2}$   
311 for the full six-year period which corresponds to 5% of total ER flux. In this calculation, parameters like  
312 decaying rates, size of PPT event, and previous soil and flux conditions were not considered (modeled) and  
313 was subjected to the number of PPT events. Logically, humid years with a greater number of PPT events have  
314 more contribution of C efflux by priming effect. Each year contributed with less than  $30 \text{ g m}^{-2} \text{ y}^{-1}$ .



315 **4. Discussion**

316 **4.1 Dynamics of the “Priming effect”**

317 In agreement with the T-D model, NEE exponentially decreased after the PPT pulse (Fig. 5) to almost the pre-  
318 PPT NEE rate. The largest C efflux pulses slowly returned to basal C efflux rates and showed larger NEE  
319 remnants than the smaller pulses (Fig. 5). This suggests that more persistent VWC quantities achieved with  
320 larger size PPT events promoted larger and longer lasting C effluxes. If the event was large enough to  
321 maintain VWC above a threshold (e.g., above the wilting point for plants) for a long time, NEE is expected to  
322 remain higher than pre-event rates until nutrients or labile C are depleted (Jarvis et al., 2007; Xu et al., 2004).  
323 In contrast, when the PPT event is small and the soil remains wet for a short-time, the C flux peak will be  
324 small and less persistent because of soil dry-out and the activity of microorganisms it is likely to end before  
325 soil nutrients are depleted. Thus, ‘priming effect’ decaying rates (-k) likely are more an issue of water  
326 availability than nutrient or C source depletion.

327 **4.2 Thresholds and time delays of the “Priming carbon flux effect”**

328 In our study, the NEE increased immediately (short-time delay) after a PPT event, in accordance with (H1).  
329 Moreover, the minimum size of an PPT event needed to detect NEE change was as low as  $0.25 \text{ mm d}^{-1}$ , in  
330 agreement with (H2). We interpret that immediate daytime PPT induced responses in NEE and ER rates were  
331 dominated by heterotrophic respiration and assume that these microbial communities have evolved to take  
332 advantage of this short-term water availability. Short-term responses of < 30-min have also been reported in  
333 studies that analyzed soil microorganism activity through molecular and stable isotope techniques (Placella et  
334 al., 20012; Unger et al., 2010). Fungi and bacteria on the soil surface have the capability for water-induced  
335 re-activation within 1 to 72-h after a PPT event (Placella et al., 2012). Immediate positive NEE increase  
336 observed in our study (Fig. A.3) may have resulted from such rapid activation of bacteria displaying highest  
337 activity 1-h after wetting. Biological soil crust (BSC) are assemblages of microorganism forming crusts on  
338 the soil and rock surfaces (Belnap, 2003) common in arid lands. At our site, the BSC covers up to 70% of  
339 plant interspaces in grazing-excluded conditions and up to 30% in overgrazed sites (Concostrina-Zubiri et al.,  
340 2014) with dominance of actinobacterias (e.g., actinomycetes) and cyanobacterias, which are identified as  
341 rapid responders (Bowling et al., 2011). Moreover, Medina-Roldán et al. (2013) at the same study site showed  
342 an increase of 36% and 34% of extractable  $\text{NH}_4^+$  and  $\text{NO}_3^-$ , respectively, after a PPT event of 10 mm.

343 The maximum priming NEE effect was identified under changes larger than 8% of soil water content at 2.5  
344 cm, previous dry soil, neutral previous NEE and PPT events > 15 mm. These limits may be defined by  
345 several conditions, including; 1) the largest and most intense events did not completely infiltrate into the soil,  
346 forming abundant runoff, and moderating the amount of water penetrating the soil profile at similar depth as  
347 that found from large-size PPT events, 2) oxygen and  $\text{CO}_2$  diffusion limitation under high soil VWC  
348 dampened soil respiration, 3) all soil aggregates are disrupted at medium soil VWC likely providing no  
349 additional nutrient or C substrate at higher VWCs (Bailey et al., 2019; Lado-Monserrat et al., 2014; Homyak  
350 et al., 2018; Chen et al., 2019), and 4) a combination of any of these three. Linear relationship between PPT



351 event size,  $\text{preVWC}_{2.5}$  and  $\Delta\text{VWC}_{2.5}$  (Fig. 2d) showed that there was not a strong limitation of water  
352 infiltration into the soil at shallow depths, discarding in some way the first condition, whereas the reduction of  
353 ER rates in nighttime NEE data after  $\text{VWC}_{2.5} > 12\%$ , and daytime  $\Delta\text{NEE}$  reductions under higher  
354  $\text{preVWC}_{2.5}$  supports the second mechanism (Fig. 6, and A4).

#### 355 4.2 The ER and GEE threshold and time delays difference

356 The smallest PPT events only stimulated ER rates, with no apparent change observed in GEE (Fig. 3). Even a  
357 large PPT event of  $20 \text{ mm d}^{-1}$  recorded in May 2013 (Fig. 3) did not induce an increase in GEE. In contrast,  
358 larger or consecutive PPT events that reached deeper soil profiles stimulated GEE (cumulative PPT  $> 40\text{mm}$ ).  
359 These results also explain why the a priori soil moisture and the change of VWC (2.5 cm depth) better  
360 explained  $\Delta\text{NEE}$  at the respiration-dominated period, rather than soil moisture at 15 cm depth (Fig 5); this  
361 confirms our notion that soil microorganism activity was the source of the immediate  $\text{CO}_2$  efflux. In contrast,  
362 VWC at 15 cm depth was the second most important factor explaining priming NEE effect in the  
363 photosynthesis-dominated period. Additionally, the change of PPFD during the photosynthesis-dominated  
364 period affected positively the priming effect (Fig. 6), it means that reduction of carbon uptake by cloudy  
365 conditions was larger than the stimulus of ecosystem respiration by the increase of soil moisture.

366 The low PPT threshold that stimulated ER agrees with results from other studies in arid ecosystems (and are  
367 even lower). PPT events as small as  $3 \text{ mm}$  induced respiration of biological soil crusts (Kurc and Small,  
368 2007), and PPT events  $< 10 \text{ mm d}^{-1}$  on a shortgrass steppe promoted net loss of C (Parton et al., 2012).  
369 However, the dominant species at our site, *B. gracilis*, was reported to respond to PPT events as small as  $5$   
370  $\text{mm}$  (Sala and Lauenroth, 1982), which was the PPT threshold we were expecting. Instead, this study found  
371 that large or consecutive PPT events had to occur before an effect on GEE was observed (Fig 3).  
372 Nevertheless, it is interesting to note that small PPT events in arid ecosystems that do not lead to C uptake  
373 may alleviate stress after severe droughts, rehydrating plant tissues and helping plants to respond faster after  
374 larger PPT events (Sala and Lauenroth, 1982; Aguirre-Gutiérrez et al., 2019).

375 Causes of larger time-delays in GEE than ER is likely due to the delay between the PPT event and the  
376 infiltration of water to a given soil layer (e.g., 15 cm depth; Fig. 2e), and the time spent for regrowing of new  
377 roots and leaves (Ogle and Reynolds, 2004). These processes promote C losses rather than C uptake in the  
378 early growing season (Huxman et al., 2004; Delgado-Balbuena et al., 2019). In contrast, ER was primarily  
379 controlled by soil moisture at shallow soil layers that moist immediately after any PPT event and may activate  
380 soil microorganism just few hours after soil wetting as discussed above.

#### 381 4.3 Influence of event size and a priori conditions

382 The magnitude of the priming effect was determined by the size of the PPT event and mainly by the  $\Delta\text{VWC}$   
383 as well as the prior condition of the ecosystem (i.e., previous C flux, and previous soil VWC). These results  
384 agree with (H3) that proposed the PPT event size and previous conditions of the semiarid grassland would  
385 control the magnitude of the “priming NEE effect”. The a priori VWC offers insight into the potential dry-



386 wet shock experienced by soil aggregates and microorganism (Haynes and Swift, 1990) and thus accounts for  
387 nutrient and labile C accumulation in soil (Bailey et al., 2019).

388 Results indicated that larger C effluxes were induced from medium amount of PPT when the previous soil  
389 conditions were dry and had a preceding value of  $NEE \sim 0$ . Several mechanisms can explain this result: i)  
390 the accumulation of nutrients and labile C into the soil (Schimel and Bennet, 2004) because low activity of  
391 microorganisms ( $NEE \sim 0$ ) under dry soil (Homyak et al., 2018), ii) if soil VWC is maintained for a long  
392 period above a threshold, then soil microbial activity exhaust labile C sources (Jarvis et al., 2007; Fierer and  
393 Schimel, 2002). Consequently, recalcitrant C sources subjected to microbial decomposition decrease  
394 mineralization rates (Van Gestel et al., 1993).

#### 395 **4.4 Importance of the priming effect in the annual C balance.**

396 We expected a significant contribution of C release from the “priming effect” to decrease the net annual C  
397 uptake of the semiarid grassland (H4). Contribution of this short-term C efflux events to annual C balances  
398 accounted for a considerable amount, but it was a small contribution if it is considered into the ecosystem  
399 respiration flux, which was almost  $3000 \text{ g m}^{-2} \text{ s}^{-1}$ . Notwithstanding its contribution is apparently low (~5% of  
400 ecosystem respiration), it is important considering that the annual C balance (NEE) is a small fraction of the  
401 difference between ER and GEE, thus, a 5% of C released represents up to 500% of the net C uptake during  
402 an almost neutral year and may turn a C sink ecosystem into a net C source. Therefore, we cannot reject H4.

#### 403 **4.5 Priming effect and climate change perspectives.**

404 The low  $\Delta SWC_{2.5}$  and PPT threshold for respiration suggests that almost all PPT events occurring in the  
405 semiarid grasslands will produce C efflux but will be limited by the characteristics of the PPT pattern and  
406 previous soil conditions at the site. Therefore, we expect that small PPT events with dry previous conditions  
407 or long inter-event periods will limit the priming effect by maintaining the system below threshold conditions.  
408 Moreover, consecutive PPT events or large PPT events should keep soil water content above a threshold that  
409 will promote C uptake by photosynthesis, which in the long term will overcome C losses from the priming  
410 effect. However, climate change scenarios forecast for the semiarid grassland in Mexico a decrease of winter  
411 PPT and the increase of storms with larger inter-event periods, which are conditions for increasing the amount  
412 of C released by the priming effect (Arca et al., 2021; Darenova et al., 2019).

413 It is necessary a further analysis of the effect of these PPT events on vegetation since productivity will also  
414 depend on PPT event size and will be modulated by previous soil conditions. Additionally, it is likely that  
415 productivity will benefit more on accumulated PPT than respiration. Still, more analysis of projected PPT  
416 scenarios is required to forecast accurately the PPT pattern under more frequent droughts, and to know if the  
417 current PPT pattern of dry-wet years will prevail. In this sense, parameterizing a model like de T-D model  
418 will provide valuable information of more accurate C effluxes from the priming effect and how it will be  
419 affected by changes of precipitation pattern. Only after that, we will be able to predict the course of the  
420 semiarid grassland as a source or sink of C under PPT pattern changes.



421 **5. Conclusions**

422 Previous soil water conditions and previous NEE were the most important factors controlling the priming  
423 effect in the semiarid grassland. The size of precipitation had an important role in explaining the priming  
424 effect but only in the respiration-dominated period. Delays between responses of change at deeper soil layer  
425 and for regrowing processes could hide relationship between precipitation and priming effect during the  
426 photosynthesis-dominated period. Importance of the priming effect in the carbon balance could be more  
427 important under forecasted changes in precipitation pattern by increasing in both frequency and intensity the  
428 dry-wet soil cycles. A further analysis of the effect of this change of precipitation patter on ecosystem  
429 productivity is necessary before we can conclude about changes in the carbon balance of the semiarid  
430 grassland.

431

432 *Author contributions.* The study was conceived by JD, TA, HL and RV. JD, TA and CAA get and processed  
433 eddy covariance data. JD, TAR, LFM implemented the method and performed the data analyses. TAR and  
434 CAA get and processed the Enhanced Vegetation Index data. TA, HL, LFM and RV helped to interpret the  
435 results. JD, TA, HL, and RV prepared the first draft, and all authors contributed to discussion of results and  
436 the revisions of the paper.

437

438 *Competing interests.* The authors declare that they have no conflict of interest.

439

440 *Availability of data.* The datasets used and/or analyzed during the current study are available from Zenodo  
441 <https://doi.org/10.5281/zenodo.7379206>

442 **Acknowledgments**

443 Authors thank INIFAP for the facilities at CENID Agricultura Familiar research site in Ojuelos, Jalisco, to  
444 carry out this study. This research was funded by SEMARNAT-CONACYT, project reference number  
445 108000, CB 2008-01 102855, CB 2013 220788 given to TA, and CONACYT CF 320641 given to JDB.  
446 HWL acknowledges the National Science Foundation (NSF) for on-going support under cooperative support  
447 agreement (EF-1029808) to Battelle. Any opinions, findings, and conclusions or recommendations expressed  
448 in this material are those of the authors and do not necessarily reflect the views of our sponsoring agencies.

449 **References**

450 Aguado-Santacruz, G. A.: Efecto de factores ambientales sobre la dinámica vegetacional en pastizales de los  
451 Llanos de Ojuelos, Jalisco: un enfoque multivariable, Colegio de Postgraduados, Chapingo, México, 155 pp.,  
452 1993.  
453 Aguirre-Gutiérrez, C. A., Holwerda, F., Goldsmith, G. R., Delgado, J., Yopez, E., Carbajal, N., Escoto-  
454 Rodríguez, M., and Arredondo, J. T.: The importance of dew in the water balance of a continental semiarid



- 455 grassland, *J. Arid Environ.*, 168, 26–35, <https://doi.org/10.1016/j.jaridenv.2019.05.003>, 2019.
- 456 Arca, V., Power, S. A., Delgado-Baquerizo, M., Pendall, E., and Ochoa-Hueso, R.: Seasonal effects of altered  
457 precipitation regimes on ecosystem-level CO<sub>2</sub> fluxes and their drivers in a grassland from Eastern Australia,  
458 *Plant Soil*, 460, 435–451, <https://doi.org/10.1007/s11104-020-04811-x>, 2021.
- 459 Bailey, V. L., Pries, C. H., and Lajtha, K.: What do we know about soil carbon destabilization?, *Environ. Res.*  
460 *Letts.*, 14, <https://doi.org/10.1088/1748-9326/ab2c11>, 2019.
- 461 Bastida, F., García, C., Fierer, N., Eldridge, D. J., Bowker, M. A., Abades, S., Alfaro, F. D., Asefaw Berhe,  
462 A., Cutler, N. A., Gallardo, A., García-Velázquez, L., Hart, S. C., Hayes, P. E., Hernández, T., Hseu, Z. Y.,  
463 Jehmlich, N., Kirchmair, M., Lambers, H., Neuhauser, S., Peña-Ramírez, V. M., Pérez, C. A., Reed, S. C.,  
464 Santos, F., Siebe, C., Sullivan, B. W., Trivedi, P., Vera, A., Williams, M. A., Luis Moreno, J., and Delgado-  
465 Baquerizo, M.: Global ecological predictors of the soil priming effect, *Nat. Commun.*, 10, 1–9,  
466 <https://doi.org/10.1038/s41467-019-11472-7>, 2019.
- 467 Belnap, J.: Microbes and microfauna associated with biological soil crusts, *Biol. Soil Crusts Struct. Funct.*  
468 *Manag.*, 167–174, 2003.
- 469 Birch, H. F.: Mineralisation of plant nitrogen following alternate wet and dry conditions, 1964.
- 470 Borken, W. and Matzner, E.: Reappraisal of drying and wetting effects on C and N mineralization and fluxes  
471 in soils, *Glob. Chang. Biol.*, 15, 808–824, <https://doi.org/10.1111/j.1365-2486.2008.01681.x>, 2009.
- 472 Bowling, D. R., Grote, E. E., and Belnap, J.: Rain pulse response of soil CO<sub>2</sub> exchange by biological soil  
473 crusts and grasslands of the semiarid Colorado Plateau, United States, *J. Geophys. Res. Biogeosciences*,  
474 <https://doi.org/10.1029/2011JG001643>, 2011.
- 475 Christensen, J. H., Hewitson, B., Busiuc, A., Chen, A., Gao, X., Held, I., Jones, R., Kolli, R. K., Kwon, W.  
476 T., Laprise, R., Magana Rueda, V., Mearns, L., Menéndez, C. G., Räisänen, J., Rinke, A., Sarr, A., and  
477 Whetton, P.: Regional Climate Projections, in: *Climate Change 2007: The Physical Science Basis.*  
478 *Contribution of Working Group I to the Fourth Assessment Report of the Intergovernmental Panel on Climate*  
479 *Change*, edited by: Solomon, S., Qin, D., Manning, M., Chen, Z., Marquis, M., Averyt, K. B., Tignor, M., and  
480 Miller, H. L., Cambridge University Press, Cambridge, United Kingdom and New York, NY, USA, 847–940,  
481 <https://doi.org/10.1080/07341510601092191>, 2007.
- 482 Chen, L., Liu, L., Qin, S., Yang, G., Fang, K., Zhu, B., Kuzyakov, Y., Chen, P., Xu, Y., and Yang, Y.:  
483 Regulation of priming effect by soil organic matter stability over a broad geographic scale, *Nat. Commun.*,  
484 10, 1–10, <https://doi.org/10.1038/s41467-019-13119-z>, 2019.
- 485 Collins, S. L., Sinsabaugh, R. L., Crenshaw, C., Green, L., Porras-Alfaro, A., Stursova, M., and Zeglin, L. H.:  
486 Pulse dynamics and microbial processes in aridland ecosystems: Pulse dynamics in aridland soils, *J. Ecol.*, 96,  
487 413–420, <https://doi.org/10.1111/j.1365-2745.2008.01362.x>, 2008.
- 488 Concostrina-Zubiri, L., Huber-Sannwald, E., Martínez, I., Flores Flores, J. L., Reyes-Agüero, J. A., Escudero,  
489 A., and Belnap, J.: Biological soil crusts across disturbance-recovery scenarios: Effect of grazing regime on  
490 community dynamics, *Ecol. Appl.*, 24, 1863–1877, <https://doi.org/10.1890/13-1416.1>, 2014.
- 491 Darenova, E., Holub, P., Krupkova, L., and Pavelka, M.: Effect of repeated spring drought and summer heavy  
492 rain on managed grassland biomass production and CO<sub>2</sub> efflux, *J. Plant Ecol.*, 10, 476–485,



- 493 <https://doi.org/10.1093/jpe/rtw058>, 2017.
- 494 Delgado-Balbuena, J., Arredondo, J. T., Loescher, H. W., Pineda-Martínez, L. F., Carbajal, J. N., and Vargas,  
495 R.: Seasonal Precipitation Legacy Effects Determine the Carbon Balance of a Semiarid Grassland, *J.*  
496 *Geophys. Res. Biogeosciences*, 124, 987–1000, <https://doi.org/10.1029/2018JG004799>, 2019.
- 497 Easterling, D. R., Meehl, G. A., Parmesan, C., Changnon, S. A., Karl, T. R., and Mearns, L. O.: Climate  
498 Extremes: Observations, Modeling, and Impacts, *Science* (80-. ), 289, 2068–2074, 2000.
- 499 Elith, J. and Leathwick, J.: Boosted regression trees for ecological modelling and prediction, *R Doc.*, 1–22,  
500 2017.
- 501 Fierer, N. and Schimel, J. P.: Effects of drying–rewetting frequency on soil carbon and nitrogen  
502 transformations, *Soil Biol. Biochem.*, 34, 777–787, [https://doi.org/10.1016/S0038-0717\(02\)00007-X](https://doi.org/10.1016/S0038-0717(02)00007-X), 2002.
- 503 Foken, T., Leuning, R., Oncley, S. R., Mauder, M., and Aubinet, M.: Corrections and Data Quality Control,  
504 in: *Eddy Covariance*, Springer Netherlands, Dordrecht, 85–131, [https://doi.org/10.1007/978-94-007-2351-1\\_4](https://doi.org/10.1007/978-94-007-2351-1_4), 2012.
- 505
- 506 Van Gestel, M., Merckx, R., and Vlassak, K.: Microbial biomass and activity in soils with fluctuating water  
507 contents, *Geoderma*, 56, 617–626, [https://doi.org/10.1016/0016-7061\(93\)90140-G](https://doi.org/10.1016/0016-7061(93)90140-G), 1993.
- 508 Haynes, R. J. and Swift, R. S.: Stability of soil aggregates in relation to organic constituents and soil water  
509 content, *J. Soil Sci.*, 41, 73–83, <https://doi.org/10.1111/j.1365-2389.1990.tb00046.x>, 1990.
- 510 Homyak, P. M., Blankinship, J. C., Slessarev, E. W., Schaeffer, S. M., Manzoni, S., and Schimel, J. P.:  
511 Effects of altered dry season length and plant inputs on soluble soil carbon, *Ecology*, 99, 2348–2362,  
512 <https://doi.org/10.1002/ecy.2473>, 2018.
- 513 Huxman, T. E., Smith, M. D., Fay, P. A., Knapp, A. K., Shaw, M. R., Loik, M. E., Smith, S. D., Tissue, D. T.,  
514 Zak, J. C., Weltzin, J. F., Pockman, W. T., Sala, O. E., Haddad, B. M., Harte, J., Koch, G. W., Schwinning,  
515 S., Small, E. E., and Williams, D. G.: Convergence across biomes to a common rain-use efficiency, *Nature*,  
516 429, 651–654, <https://doi.org/10.1038/nature02561>, 2004a.
- 517 Huxman, T. E., Snyder, K. A., Tissue, D., Leffler, A. J., Ogle, K., Pockman, W. T., Sandquist, D. R., Potts, D.  
518 L., and Schwinning, S.: Precipitation pulses and carbon fluxes in semiarid and arid ecosystems, *Oecologia*,  
519 141, 254–268, <https://doi.org/10.1007/s00442-004-1682-4>, 2004b.
- 520 Jarvis, P., Rey, A., Petsikos, C., Wingate, L., Rayment, M., Pereira, J., Banza, J., David, J., Miglietta, F.,  
521 Borghetti, M., Manca, G., and Valentini, R.: Drying and wetting of Mediterranean soils stimulates  
522 decomposition and carbon dioxide emission: the “Birch effect,” *Tree Physiol.*, 27, 929–940, 2007.
- 523 Kim, D.-G., Vargas, R., Bond-Lamberty, B., and Turetsky, M. R.: Effects of soil rewetting and thawing on  
524 soil gas fluxes: a review of current literature and suggestions for future research, *Biogeosciences*, 9, 2459–  
525 2483, <https://doi.org/10.5194/bg-9-2459-2012>, 2012.
- 526 Knapp, A. K., Hoover, D. L., Wilcox, K. R., Avolio, M. L., Koerner, S. E., La Pierre, K. J., Loik, M. E., Luo,  
527 Y., Sala, O. E., and Smith, M. D.: Characterizing differences in precipitation regimes of extreme wet and dry  
528 years: Implications for climate change experiments, *Glob. Chang. Biol.*, 21, 2624–2633,  
529 <https://doi.org/10.1111/gcb.12888>, 2015.
- 530 Kurc, S. A. and Small, E. E.: Dynamics of evapotranspiration in semiarid grassland and shrubland ecosystems



- 531 during the summer monsoon season, central New Mexico, *Water Resour. Res.*, 40, W09305, 2004.
- 532 Lado-Monserrat, L., Lull, C., Bautista, I., Lidon, A., and Herrera, R.: Soil moisture increment as a controlling  
533 variable of the “Birch effect”. Interactions with the pre-wetting soil moisture and litter addition, *Plant Soil*,  
534 379, 21–34, <https://doi.org/10.1007/s11104-014-2037-5>, 2014.
- 535 Lal, R.: Carbon Sequestration in Dryland Ecosystems, *Environ. Manage.*, 33, 528–544,  
536 <https://doi.org/10.1007/s00267-003-9110-9>, 2004.
- 537 Lauenroth, W. K. and Sala, O. E.: Long-term forage production of North American shortgrass steppe,  
538 <https://doi.org/10.2307/1941874>, 1992.
- 539 Loescher, H. W., Law, B. E., Mahrt, L., Hollinger, D. Y., Campbell, J., and Wofsy, S. C.: Uncertainties in,  
540 and interpretation of, carbon flux estimates using eddy covariance techniques, *J. Geophys. Res.*, 111, 19,  
541 <https://doi.org/10.1029/2005JD006932>, 2006.
- 542 Loik, M. E., Breshears, D. D., Lauenroth, W. K., and Belnap, J.: A multi-scale perspective of water pulses in  
543 dryland ecosystems: Climatology and ecohydrology of the western USA, *Oecologia*, 141, 269–281,  
544 <https://doi.org/10.1007/s00442-004-1570-y>, 2004.
- 545 Maliva, R. and Missimer, T.: *Microgravity*, Springer Berlin Heidelberg, 329–342, 2012.
- 546 Massman, W. J.: A simple method for estimating frequency response corrections for eddy covariance  
547 systems, *Agric. For. Meteorol.*, 104, 185–198, [https://doi.org/10.1016/S0168-1923\(00\)00164-7](https://doi.org/10.1016/S0168-1923(00)00164-7), 2000.
- 548 Medina-Roldán, E., Arredondo Moreno, J. T., García Moya, E., and Huerta Martínez, F. M.: Soil Water  
549 Content Dynamics Along a Range Condition Gradient in a Shortgrass Steppe, *Rangel. Ecol. Manag.*, 60, 79–  
550 87, <https://doi.org/10.2111/05-219R2.1>, 2007.
- 551 Noy-Meir, I.: Desert Ecosystems: Environment and Producers, *Annu. Rev. Ecol. Syst.*, 4, 25–51, 1973.
- 552 Ocheltree, T. W. and Loescher, H. W.: Design of the AmeriFlux portable eddy covariance system and  
553 uncertainty analysis of carbon measurements, *J. Atmos. Ocean. Technol.*, 24, 1389–1406,  
554 <https://doi.org/10.1175/JTECH2064.1>, 2007.
- 555 Ogle, K. and Reynolds, J. F.: Plant responses to precipitation in desert ecosystems: integrating functional  
556 types, pulses, thresholds, and delays, *Oecologia*, 141, 282–294, <https://doi.org/10.1007/s00442-004-1507-5>,  
557 2004.
- 558 Parton, W., Morgan, J., Smith, D., Del Grosso, S., Prihodko, L., LeCain, D., Kelly, R., and Lutz, S.: Impact of  
559 precipitation dynamics on net ecosystem productivity, *Glob. Chang. Biol.*, 18, 915–927,  
560 <https://doi.org/10.1111/j.1365-2486.2011.02611.x>, 2012.
- 561 Placella, S. A., Brodie, E. L., and Firestone, M. K.: Rainfall-induced carbon dioxide pulses result from  
562 sequential resuscitation of phylogenetically clustered microbial groups, *Proc. Natl. Acad. Sci.*, 109, 10931–  
563 10936, <https://doi.org/10.1073/pnas.1204306109>, 2012.
- 564 Reichmann, L. G., Sala, O. E., and Peters, D. P. C.: Water controls on nitrogen transformations and stocks in  
565 an arid ecosystem, *Ecosphere*, 4, 1–17, <https://doi.org/10.1890/ES12-00263.1>, 2013.
- 566 Reichstein, M., Falge, E., Baldocchi, D., Papale, D., Aubinet, M., Berbigier, P., Bernhofer, C., Buchmann, N.,  
567 Gilmanov, T., Granier, A., Grünwald, T., Havránková, K., Ilvesniemi, H., Janous, D., Knohl, A., Laurila, T.,  
568 Lohila, A., Loustau, D., Matteucci, G., Meyers, T., Miglietta, F., Ourcival, J. M., Pumpanen, J., Rambal, S.,





569 Rotenberg, E., Sanz, M., Tenhunen, J., Seufert, G., Vaccari, F., Vesala, T., Yakir, D., and Valentini, R.: On  
570 the separation of net ecosystem exchange into assimilation and ecosystem respiration: Review and improved  
571 algorithm, <https://doi.org/10.1111/j.1365-2486.2005.001002.x>, 2005.

572 Ruimy, A., Jarvis, P. G., Baldocchi, D. D., Saugier, B., and M. Begon and A.H. Fitter: CO<sub>2</sub> Fluxes over Plant  
573 Canopies and Solar Radiation: A Review, vol. Volume 26, Academic Press, 1–68, 1995.

574 Sala, O. E. and Lauenroth, W. K.: Small rainfall events: An ecological role in semiarid regions, *Oecologia*,  
575 53, 301–304, <https://doi.org/10.1007/BF00389004>, 1982.

576 Schotanus, P., Nieuwstadt, F. T. M., and De Bruin, H. A. R.: Temperature measurement with a sonic  
577 anemometer and its application to heat and moisture fluxes, *Boundary-Layer Meteorol.*, 26, 81–93,  
578 <https://doi.org/10.1007/BF00164332>, 1983.

579 Turner, B. and Haygarth, P. M.: Phosphorus solubilization in rewetted soils, *Nature*, 411, 258,  
580 [https://doi.org/10.1002/\(SICI\)1097-0177\(199909\)216:1<1::AID-DVDY1>3.0.CO;2-T](https://doi.org/10.1002/(SICI)1097-0177(199909)216:1<1::AID-DVDY1>3.0.CO;2-T), 2001.

581 Webb, E. K., Pearman, G. I., and Leuning, R.: Correction of flux measurements for density effects due to heat  
582 and water vapour transfer, <https://doi.org/10.1002/qj.49710644707>, January 1980.

583 Xu, L., Baldocchi, D. D., and Tang, J.: How soil moisture, rain pulses, and growth alter the response of  
584 ecosystem respiration to temperature, *Global Biogeochem. Cycles*, 18, n/a-n/a,  
585 <https://doi.org/10.1029/2004GB002281>, 2004.

586 Yang, X., Tang, J., and Mustard, J. F.: Beyond leaf color: Comparing camera-based phenological metrics with  
587 leaf biochemical, biophysical, and spectral properties throughout the growing season of a temperate deciduous  
588 forest, *J. Geophys. Res. Biogeosciences*, 119, 181–191, <https://doi.org/10.1002/2013JG002460>, 2014.

589  
590



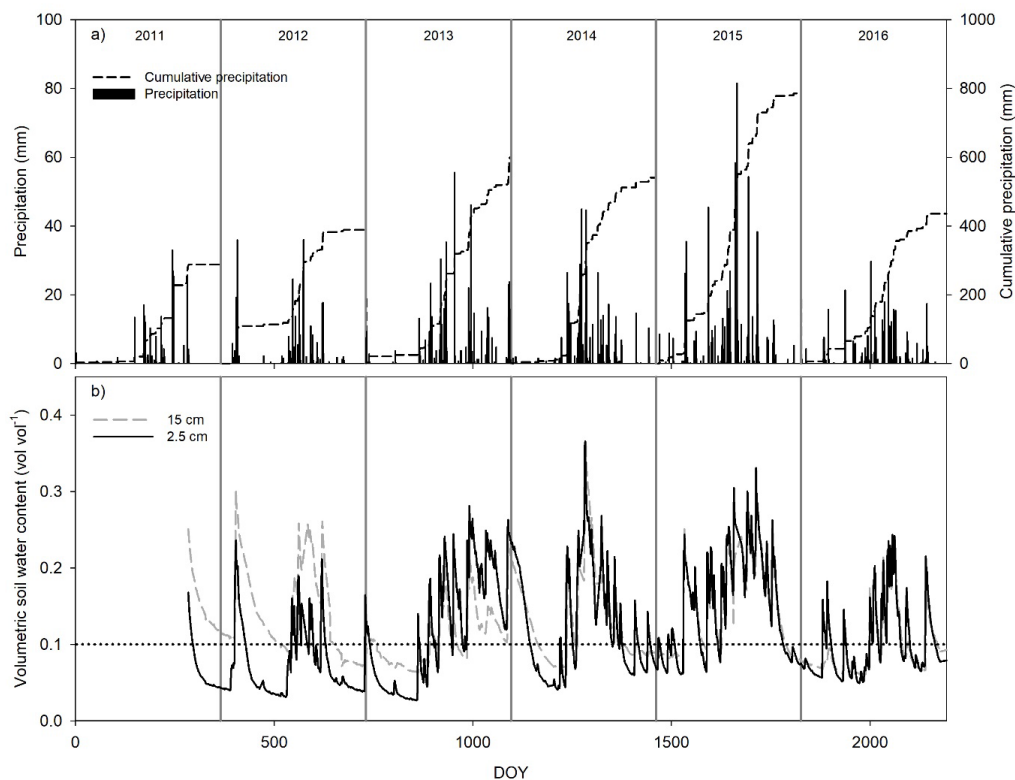
591 **Table 1. Relative importance (RI) of the first four most important environmental factors for the “priming CO<sub>2</sub>**  
592 **effect”.**

	RI
Respiration-dominated period	
$\Delta\text{VWC}_{2.5}$	18.66
preNEE	14.67
preVWC <sub>2.5</sub>	14.08
PPT	13.64
preVWC <sub>15</sub>	8.09
VWC <sub>2.5</sub>	7.46
Photosynthesis-dominated period	
preNEE	33.32
VWC <sub>15</sub>	12.25
$\Delta\text{PPFD}$	11.52
VWC <sub>2.5</sub>	9.16
Tair	8.32
preVWC <sub>2.5</sub>	7.79

593

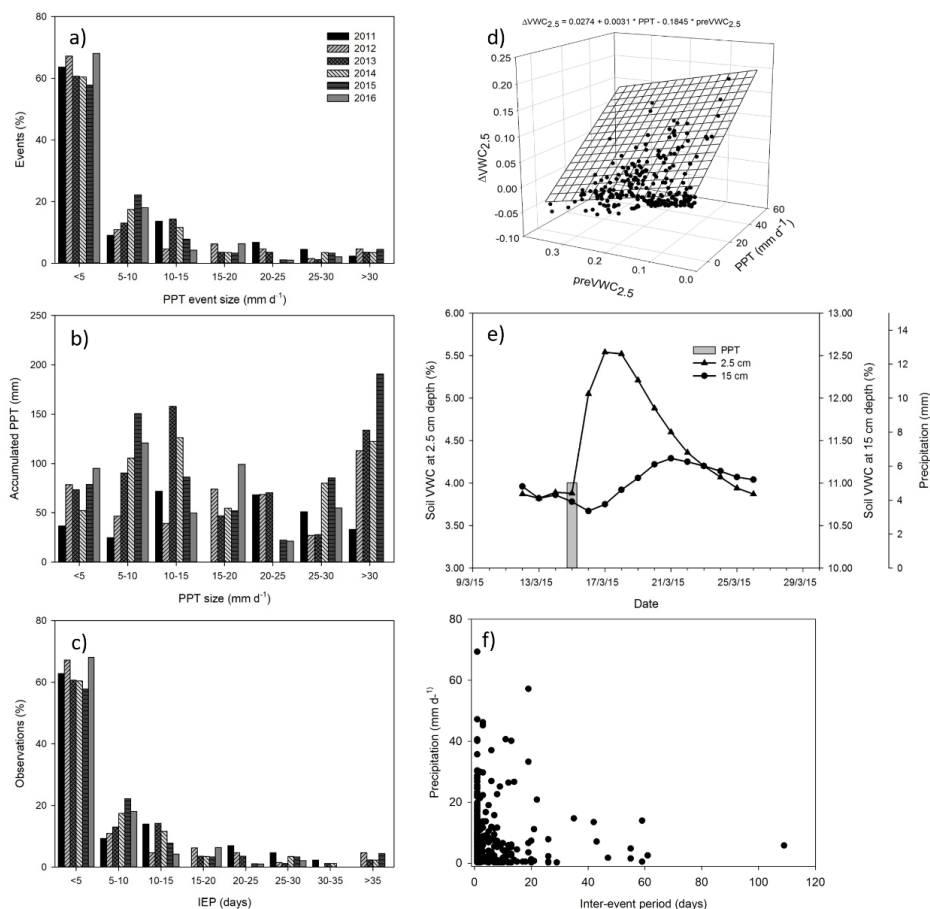
594

595



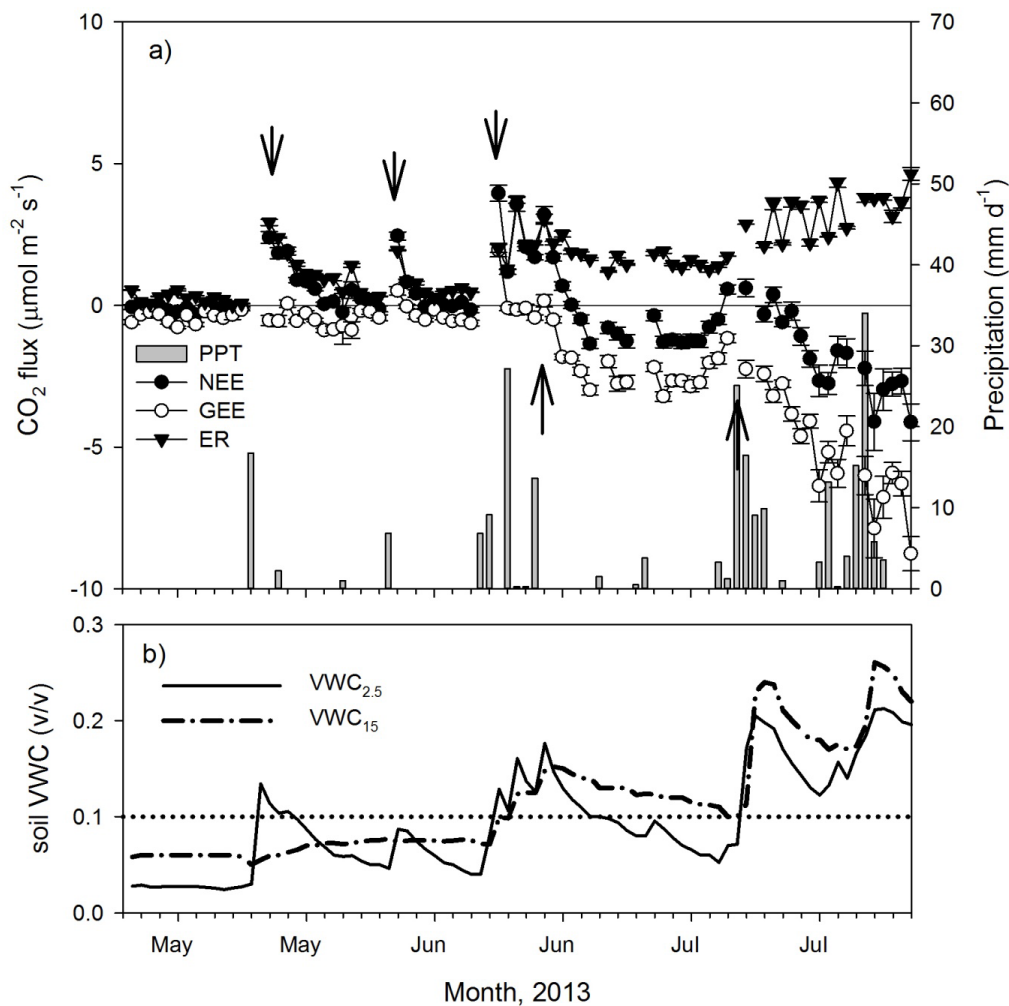
596

597 **Figure 1. Seasonal and interannual variation of daily precipitation and cumulative precipitation (a), and**  
598 **volumetric soil water content at 2.5 (black line) and 15 cm depth (gray line; b). Dotted line at 10% of soil water**  
599 **content was depicted as reference.**



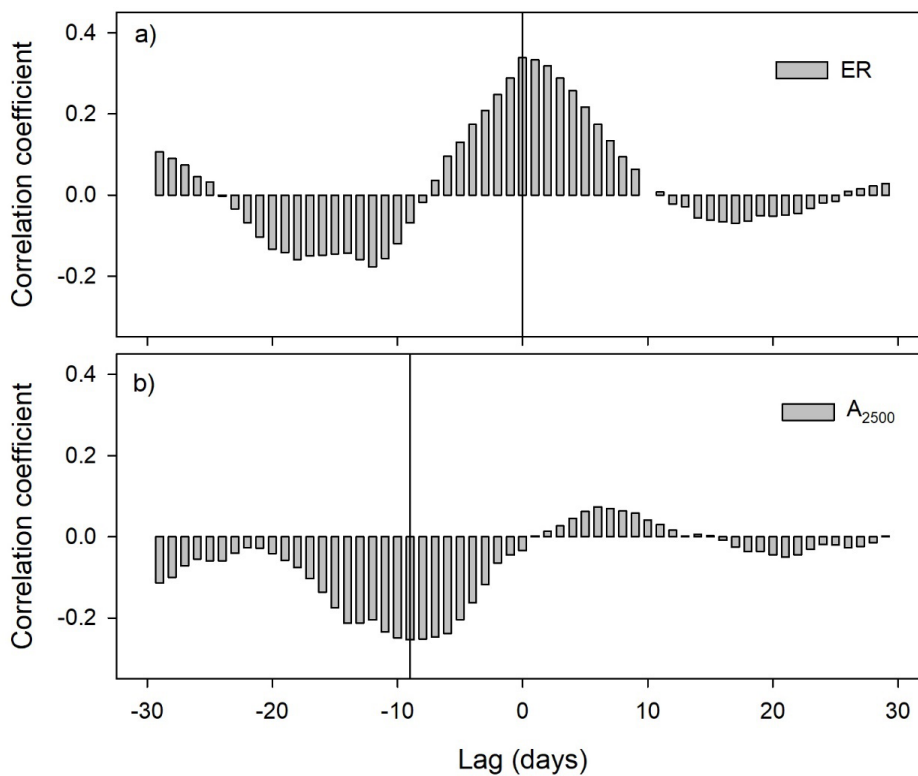
600

601 **Figure 2. Characterization of precipitation pattern. Histogram of the size of precipitation events through six years**  
 602 **(a), the accumulated precipitation by size of precipitation event (b), and the number (%) of precipitation events by**  
 603 **inter-event period classes (IEP, days; c). Relationship between size of precipitation event ( $mm\ d^{-1}$ ), previous**  
 604 **volumetric soil water content at 2.5 cm depth ( $v/v$ ) and the change in soil volumetric water content at 2.5 cm depth**  
 605 **( $v/v$ ). Dynamic of soil water content at two depths (2.5 and 15 cm) after a precipitation event of 5 mm through the**  
 606 **time (e), and relationship between inter-event period and the size of precipitation event (f).**



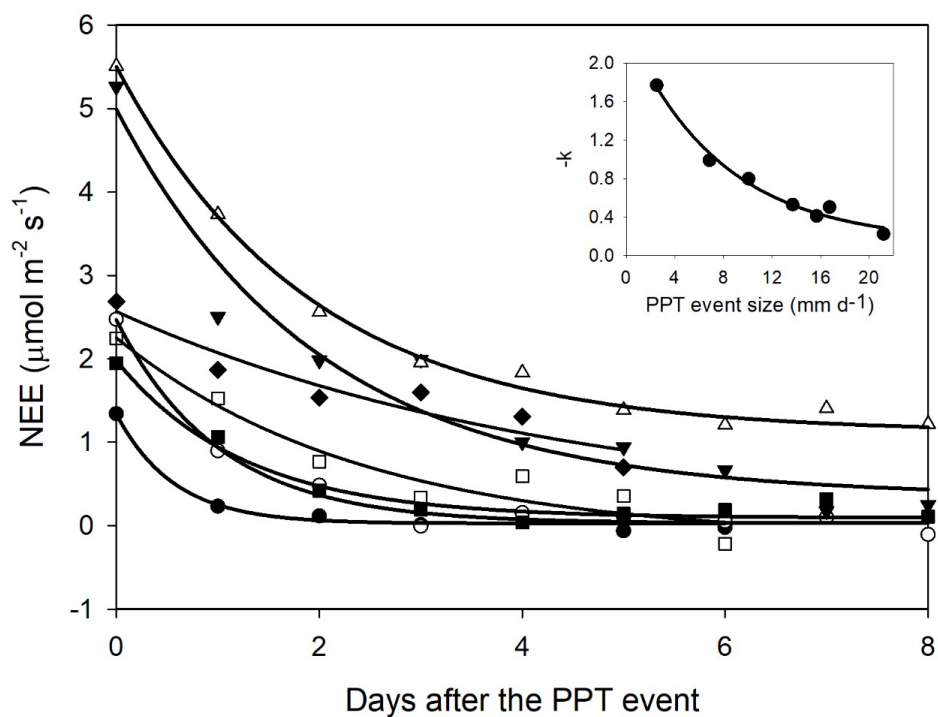
607

608 Figure 3. Dynamics of a) precipitation ( $\text{mm d}^{-1}$ ) and net ecosystem exchange (NEE,  $\mu\text{mol m}^{-2} \text{s}^{-1}$ , daily means  $\pm 1$   
609 SE) and its components, the gross ecosystem exchange (GEE,  $\mu\text{mol m}^{-2} \text{s}^{-1}$ ) and ecosystem respiration (ER,  $\mu\text{mol m}^{-2} \text{s}^{-1}$ ) for the transition from the dry (December – May) to the wet season (June – November) in 2013. b) volumetric  
610 soil water content dynamics (VWC, v/v) at two depths (2.5 cm and 15 cm). Arrows indicate apparent changes in  
611 GEE and ER trends. Dotted line indicates SWC = 0.1.  
612



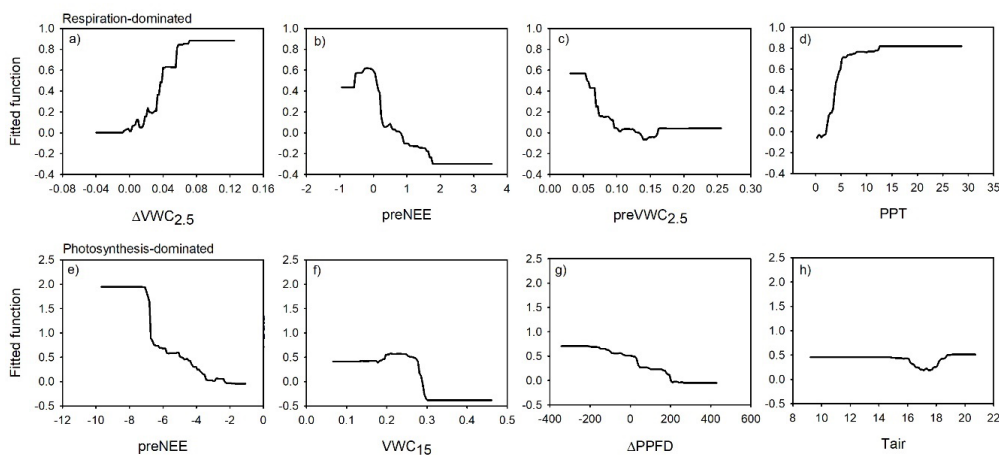
613

614 **Figure 4.** Cross-correlation coefficients between detrended time series of soil water content at 2.5 cm depth and  
615 ecosystem respiration (ER, a), and between soil water content at 15 cm depth and photosynthesis at 2500  $\mu\text{mol m}^{-2}$   
616  $\text{s}^{-1}$  of photosynthetic photon flux density ( $A_{2500}$ ; b).



617

618 Figure 5. Net ecosystem exchange (NEE) after a precipitation event showing the decreasing effect through time  
619 (days). The decreasing effect rate was adjusted to an exponential negative model  $NEE = y_0 + a \cdot \exp(-k \cdot t)$ . The  
620 insert stands for the relationship between the decaying rate ( $-k$ ) and the PPT event that originated the NEE change.  
621 This relationship was fitted with an exponential model (black line;  $-k = y_0 + a \cdot \exp(-b \cdot PPT\_event)$ ). Symbols  
622 indicate different PPT event sizes that originated the NEE change,  $13.7 \text{ mm d}^{-1}$  ( $\Delta$ ),  $16.74 \text{ mm d}^{-1}$  ( $\blacktriangledown$ ),  $6.86 \text{ mm d}^{-1}$   
623 ( $\circ$ ),  $10.08 \text{ mm d}^{-1}$  ( $\blacksquare$ ),  $2.52 \text{ mm d}^{-1}$  ( $\bullet$ ),  $21.18 \text{ mm d}^{-1}$  ( $\square$ ), and  $15.68 \text{ mm d}^{-1}$  ( $\blacklozenge$ ).



624

625 **Figure 6.** Fitted functions of the boosted regression trees between the “priming CO<sub>2</sub> effect” and the four most  
626 important environmental variables at ecosystem respiration-dominated period (upper panel) and at the  
627 photosynthesis-dominated period (bottom panel). Priming effect ( $\Delta NEE$ ,  $\mu\text{mol m}^{-2} \text{s}^{-1}$ ); previous NEE (preNEE,  
628  $\mu\text{mol m}^{-2} \text{s}^{-1}$ ); previous VWC at 2.5 cm depth (preVWC<sub>2.5</sub>, v/v); PPT event size (PPT, mm); VWC at 15 cm depth  
629 (VWC<sub>15</sub>, v/v); change of photosynthetic photon flux density ( $\Delta\text{PPFD}$ ,  $\mu\text{mol m}^{-2} \text{s}^{-1}$ ); air temperature ( $T_{\text{air}}$ , °C).

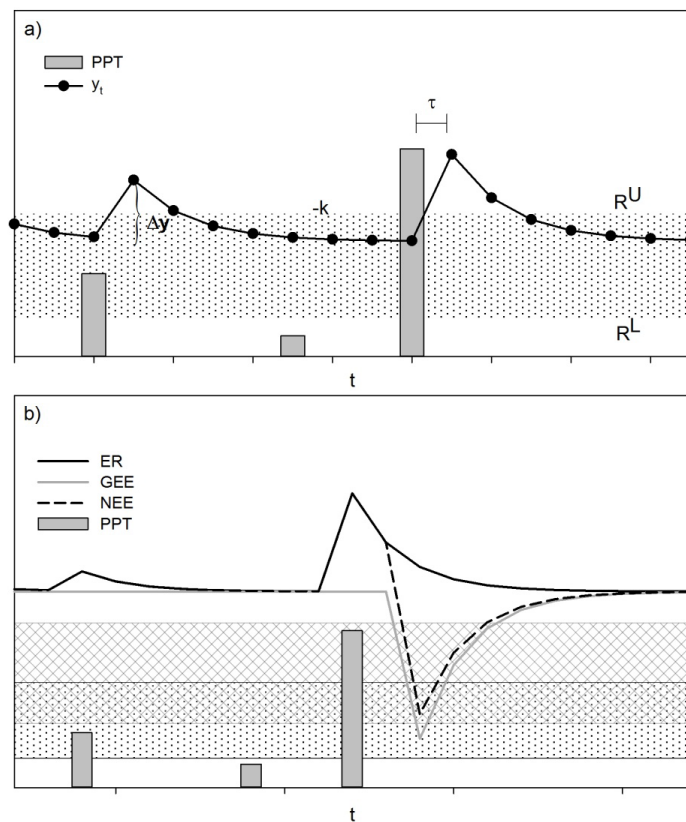
630

631





632 **Appendix A. Ancillary figures**

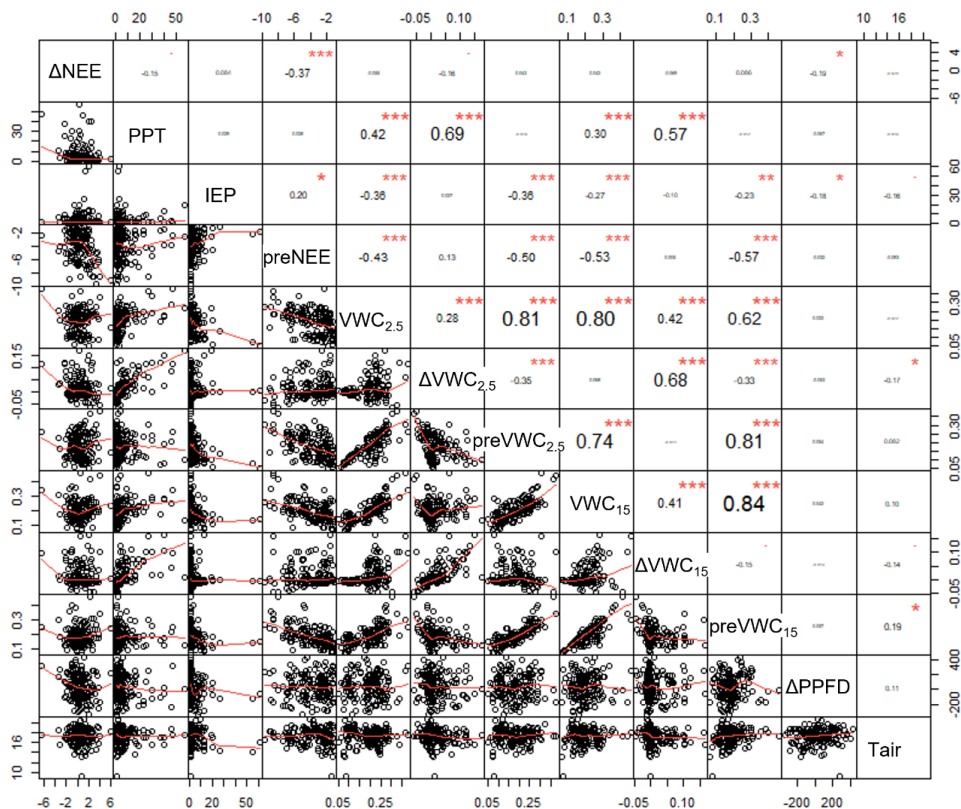


633

634 **Figure A1.** The Threshold-Delay model (Ogle and Reynolds, 2004). a) The magnitude of the increase in the  
635 response variable ( $\Delta t$ , e.g., carbon flux,  $y_t$ ) is determined by the size of PPT event and by the previous state of  
636 the response variable. The decreasing rate of the response following the stimulus is denoted by  $-k$ . The low  
637 PPT threshold ( $R^L$ ) indicates the minimum size PPT event to stimulate a response, and the upper PPT  
638 threshold ( $R^U$ ) indicates PPT events that do not cause additional increment in the response variable. The time  
639 interval between the stimulus and the response is described by  $\tau$ . b) The response of the net ecosystem  
640 exchange (NEE), that is the balance between the gross ecosystem exchange (GEE) and ecosystem respiration  
641 (ER), vary in response to changes of GEE and ER. According to the T-D model, GEE and ER have different  
642 PPT thresholds (dotted band and mesh stand for effective PPT events size for ER and GEE, respectively), with

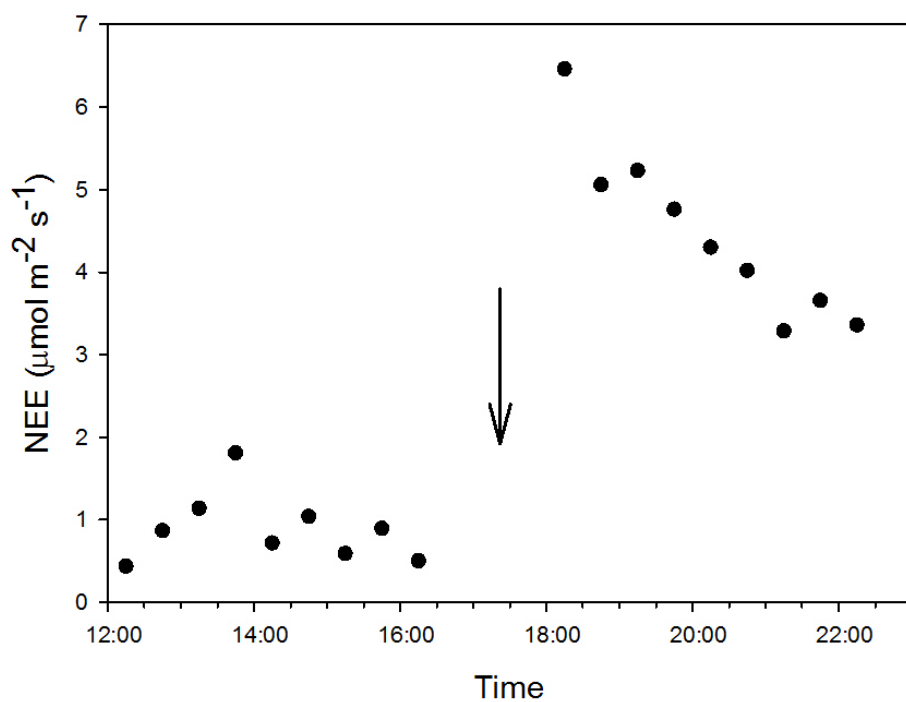


643 ER responding to smaller size PPT events than GEE, therefore, small PPT events favor C release whereas  
644 large PPT events stimulate net C uptake by the ecosystem. Differences of time responses between soil  
645 microorganisms and plants to soil wet up led GEE and ER to differ in time delays ( $\tau$ ), with shorter time delays  
646 for ER than GEE (Huxman et al., 2004a). The hypothetical curve for NEE and its components was calculated  
647 introducing arbitrary parameters in the T-D model equations of Ogle and Reynolds (2004).



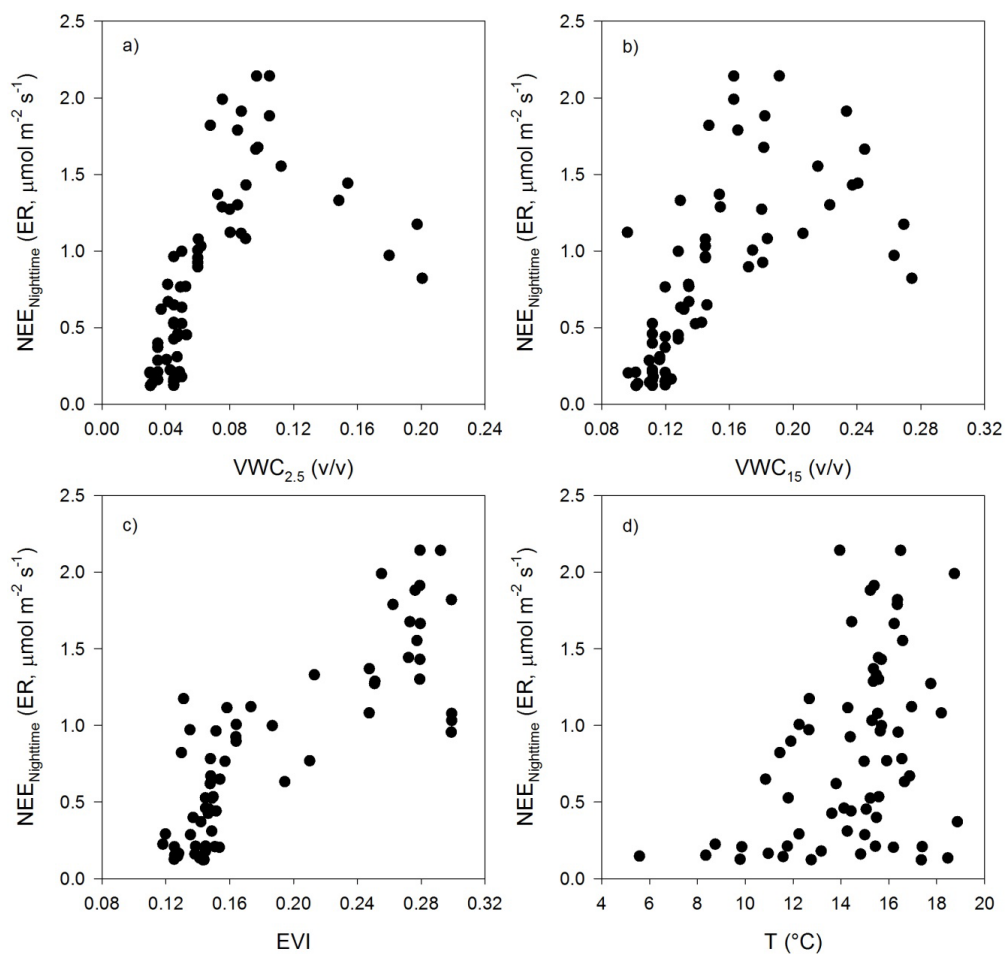
648

649 **Figure A2.** Correlation matrix among all variables.



650

651 **Figure A3.** Dynamic of half an hour net ecosystem exchange ( $\mu\text{mol m}^{-2} \text{s}^{-1}$ ) after a precipitation event of 8.12  
652 mm. The arrow indicates the time of PPT event occurrence.



653

654 **Figure A4.** Relationship between nighttime-NEE derived ER and a) the soil volumetric water content at 2.5  
655 cm depth (VWC<sub>2.5</sub>, v/v), b) the soil volumetric water content at 15 cm depth (VWC<sub>15</sub>, v/v), c) the enhanced  
656 vegetation index (EVI), and d) the air temperature (T, °C).